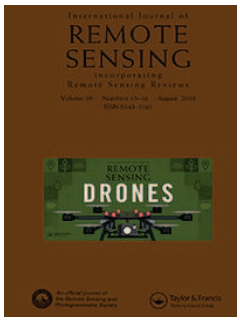

International Journal of Remote Sensing

ISSN: 0143-1161 (Print) 1366-5901 (Online) Journal homepage: https://www.tandfonline.com/loi/tres20

Comparison of ALS- and UAV(SfM)-derived high-density point clouds for individual tree detection in Eucalyptus plantations

Juan Guerra-Hernández, Diogo N. Cosenza, Luiz Carlos Estraviz Rodriguez, Margarida Silva, Margarida Tomé, Ramón A. Díaz-Varela & Eduardo González-Ferreiro

To cite this article: Juan Guerra-Hernández, Diogo N. Cosenza, Luiz Carlos Estraviz Rodriguez, Margarida Silva, Margarida Tomé, Ramón A. Díaz-Varela & Eduardo González-Ferreiro (2018) Comparison of ALS- and UAV(SfM)-derived high-density point clouds for individual tree detection in Eucalyptus plantations, International Journal of Remote Sensing, 39:15-16, 5211-5235, DOI: 10.1080/01431161.2018.1486519

To link to this article: https://doi.org/10.1080/01431161.2018.1486519

Published online: 03 Jul 2018.

INTERNATIONAL JOURNAL OF REMOTE SENSING
2018, VOL. 39, NOS. 15–16, 5211–5235
https://doi.org/10.1080/01431161.2018.1486519

Taylor & Francis
Taylor & Francis Group

Comparison of ALS- and UAV(SfM)-derived high-density point clouds for individual tree detection in Eucalyptus plantations

Juan Guerra-Hernández[a], Diogo N. Cosenza[a], Luiz Carlos Estraviz Rodriguez[b], Margarida Silva[c], Margarida Tomé[a], Ramón A. Díaz-Varela[d] and Eduardo González-Ferreiro[e,f]

[a]Forest Research Centre (CEF), Instituto Superior de Agronomía, University of Lisbon, Lisboa, Portugal; [b]Grupo de Estudos em Tecnologias LiDAR (GET-LiDAR), Departamento de Ciências Florestais, Escola Superior de Agricultura "Luiz de Queiroz", Universidade de São Paulo (SPU), Piracicaba, Brazil; [c]RAIZ (Forest and Paper research Institute), The Navigator Company, Eixo, Portugal; [d]Departamento de Botánica, Biodiversidade e Botánica Aplicada, Grupo de Investigación en Biodiversidade e Botánica Aplicada GI-1809-BIOAPLIC, Escola Politécnica Superior, Universidade de Santiago de Compostela, R/ Benigno Ledo s/n, Campus Terra, 27002 Lugo, España; [e]Departamento de Producción Vexetal e Proxectos de Enxeñaría, Unidade de Xestión Forestal Sostible GI-1837-UXFS, Escola Politécnica Superior, Universidade de Santiago de Compostela, R/ Benigno Ledo s/n, Campus Terra, 27002 Lugo, España; [f]Departamento de Tecnología Minera, Topografía y de Infraestructuras, Grupo de Investigación en Geomática e Ingeniería Cartográfica GI-202-GEOINCA, Escuela Superior y Técnica de Ingenieros de Minas, Universidad de León, Av. de Astorga s/n, Campus de Ponferrada, 24401 Ponferrada, España

ABSTRACT

Highly accurate, rapid forest inventory techniques are needed to enable forest managers to address the increasing demand for sustainable forestry. In the last two decades, Airborne Laser Scanning (ALS) and Terrestrial Laser Scanning have become internationally established as forest mapping and monitoring methods. However, recent advances in sensors and in image processing – particularly Structure from Motion (SfM) technology – have also enabled the extraction of dense point clouds from images obtained by Digital Aerial Photography (DAP). DAP is cheaper than ALS, especially when the systems are mounted on small unmanned aerial vehicles (UAVs), and the density of the point cloud can easily reach the levels yielded by ALS devices. The main objective of this study was to evaluate and compare the usefulness of ALS-derived and UAV(SfM)-derived high-density point clouds for detecting and measuring individual tree height in *Eucalyptus* spp. plantations established on complex terrain. A total of 325 reference trees were measured and located in 6 square plots (400 m^2). The individual tree crown (ITC) delineation algorithm detected 311 from the ALS-derived data and 259 trees from the UAV (SfM)-derived data, representing accuracy levels of, respectively, 96% and 80%. The results suggest that at plot level, UAV(SfM)-generated point clouds are as good as ALS-derived point clouds for estimating individual tree height. Furthermore, analysis of the differences in digital elevation models at landscape level showed that the elevations of the UAV(SfM)-derived terrain surfaces were slightly higher than the ALS-derived surfaces (mean difference, 1.14 m and standard deviation, 1.93 m). Finally, we discuss how non-optimal UAV-image-

ARTICLE HISTORY
Received 22 December 2017
Accepted 30 May 2018

CONTACT Juan Guerra-Hernández juanguerra@isa.ulisboa.pt Forest Research Centre (CEF), University of Lisbon, Tapada da Ajuda, 1349-017 Lisboa, Portugal

acquisition conditions and slope terrain affect the ITC delineation process.

1. Introduction

The availability of accurate information on forest resources has a decisive impact on decision-making processes in forest and timber management. Forest inventory data are used to determine the current state of the forest and future projections, and they also allow correct allocation of forest stocks in both spatial and temporal dimensions. Most management decisions require precise knowledge about forest structure.

In the past two decades, airborne laser scanning (ALS) has become the preferred remote-sensing technique for individual tree crown (ITC) delineation, mainly because it can quickly provide highly accurate and spatially detailed information about forest attributes across an entire forested landscape (Hyyppä and Inkinen 1999; Lim et al. 2003). ALS technology, also referred to as airborne lidar (light detection and ranging), combines accurate distance measurements with laser light, Global Navigation Satellite System (GNSS) positioning and precise orientation with an inertial measurement unit (IMU). The technology enables acquisition of spatially accurate three-dimensional (3D) point clouds that represent the shape of the scanned objects. The use of ALS-derived point clouds has proved to be an accurate means of determining forest canopy structure (e.g. Lim et al. 2003).

The photogrammetry has long been used for assessing forest resources (Durrieu et al. 2015), and for example, photogrammetry-based 3D measurements of tree height have been conducted since the 1940s (see Korpela 2004). Use of stereophotogrammetry and detection of common points (e.g. a tree top) on at least two images enables the 3D coordinates (*XYZ*) to be defined. However, advances in sensor technology and image processing have led to generation of dense Digital Aerial Photography (DAP)-based point clouds of similar densities to those provided by ALS. The DAP-based point clouds are generated using automatic image matching algorithms, e.g. by semi-global matching (Hirschmuller 2005). The density of the final point cloud depends on the image resolution and the matching algorithm used (Baltsavias et al. 2008; St-Onge et al. 2008; White et al. 2013). In the field of forestry, DAP-based point clouds can be used to predict forest stand attributes in the same way as ALS-based point clouds (Bohlin, Wallerman, and Fransson 2012; Vastaranta et al. 2013; Rahlf et al. 2014; Holopainen et al. 2015; Puliti, Gobakken et al. 2017). Nowadays, researchers use Structure from Motion (SfM) and multi-view stereopsis techniques to process large amounts of imaging data. Unlike traditional DAP-based methods, these techniques do not require information about the position of the camera or multiple control points (Westoby et al. 2012; Tomaštík et al. 2017). Thus, SfM enables the rapid extraction of 3D information from unmanned aerial vehicle (UAV) flights based on feature matching with overlapping images (Fritz, Kattenborn, and Koch 2013; Zarco-Tejada et al. 2014; Díaz-Varela et al. 2015).

Two main methods of assessing forest attributes by using ALS and DAP data can be distinguished. The area-based approach (ABA) provides various statistical features to describe the canopy structure on the basis of the 3D point clouds coordinates. Low-density ALS data (<1 point m^{-2}) are typically used in the ABA approach (Naesset 1997;

Næsset 2002; Guerra-Hernández et al. 2016). The second approach, referred to as the individual tree-based approach, is based on ITC delineation and usually uses more dense ALS point clouds (>5 point m^{-2}) than ABA (Hyyppä et al. 2008). This method is based on the identification of those points in the cloud that correspond to and represent each ITC so that individual tree level features can then be derived from the trees detected (Hyyppä and Inkinen 1999; González-Ferreiro et al. 2013; Díaz-Varela et al. 2015; Guerra-Hernández et al. 2017).

The use of UAVs to acquire ALS- and DAP-derived images has increased greatly during the past five years (Wallace et al. 2012; Lisein et al. 2013; Wallace et al. 2016; Jaakkola et al. 2017). Advances in UAV technology and data processing methods have made it feasible to obtain high-resolution imagery and 3D data that can be used for forest monitoring and for assessing tree attributes (Dandois and Ellis 2010; Lisein et al. 2013; Dandois, Olano, and Ellis 2015; Puliti et al. 2015). The use of light UAVs (drones) equipped with inexpensive consumer grade cameras has recently emerged as a feasible option for monitoring forest structure, especially because of the low cost and operational flexibility of the systems (Goodbody, Coops, Hermosilla et al. 2017; Puliti, Ene et al. 2017; Guerra-Hernández et al. 2017). Recent scientific studies have demonstrated the increasing capacity of user-friendly, versatile, and inexpensive UAVs for measuring tree height and biomass growth in the short term, thus leading to novel practical applications in forestry and research (Goodbody, Coops, Marshall et al. 2017; Dempewolf et al. 2017; Jiménez-Brenes et al. 2017; Guerra-Hernández et al. 2017).

In terms of forest resource assessment, there are strengths and weaknesses in the collection of both ALS- and DAP-based data (White et al. 2013, 2015, 2016). Although highly dependent on the data density, the cost of acquiring DAP data is between approximately a third and a half of the cost of acquiring ALS data (Nurminen et al. 2013; White et al. 2013; Holopainen et al. 2015). DAP-derived images might also provide additional high-resolution spectral information and can be used together with the extracted point cloud, e.g. for species classification (Ahmed et al. 2017; Franklin and Ahmed 2017). Recent developments in image processing have made it possible to generate point clouds of sufficiently high density for ITC delineation, by using UAV-based DAP combined with ALS-derived DEMs in densely forested areas (Goodbody, Coops, Marshall et al. 2017b) or by using only the DEM directly derived from UAV-based DAP in open canopy areas (Jensen and Mathews 2016; Guerra-Hernández et al. 2017; Kachamba et al. 2017). Nevertheless, UAV-based DAP has several limitations: (1) fewer flying hours per day are possible than with ALS, which is insensitive to shadows of clouds (White et al. 2013); (2) the images are strongly influenced by atmospheric conditions, solar illumination, and view angles (Sun, surface, and sensor geometry); occlusions caused by shadows are particular problematic for generation of image-based point clouds in dense forest canopies (Baltsavias 1999; Laliberte et al. 2010; Ke and Quackenbush 2011; Dandois, Olano, and Ellis 2015; Simic Milas et al. 2017), and (3) the low capacity to generate accurate DEMs under vegetation canopy, which is one of the most commonly cited drawbacks of DAP-based point clouds (White et al. 2015).

In recent years, UAV-based forestry applications of both ALS and DAP have increased (Torresan et al. 2017; Thiel and Schmullius 2017; Bonnet, Lisein, and Lejeune 2017). ALS-derived canopy height models (CHMs) can be used to detect individual trees, delineate tree crowns, and subsequently to estimate biophysical attributes such as biomass and stem volume (Popescu, Wynne, and Nelson 2003; Popescu 2007; Falkowski et al. 2008,

2009; Silva et al. 2016). In the same way, UAV-based DAP studies have focused on exploring the use of SfM-derived CHMs, suggesting their potential to estimate individual-tree variables such as height and diameter at breast height via tree-top detection and crown delineation (Díaz-Varela et al. 2015; Panagiotidis et al. 2017; Guerra-Hernández et al. 2017). A variety of approaches are used to detect and delineate individual trees from ALS- and SfM-derived CHMs. These include the identification of local maxima for tree detection (Popescu, Wynne, and Nelson 2003; Falkowski et al. 2008, 2009), as well as region-growing (Hyyppa et al. 2001; Solberg, Naesset, and Bollandsas 2006), valley-following (Leckie et al. 2003), and watershed segmentation (González-Ferreiro et al. 2013; Díaz-Varela et al. 2015) for delineation.

Recent studies have compared the performance of both technologies both separately and in combination for characterizing forest tree height (Wallace et al. 2016; Thiel and Schmullius 2017) or residual volume after harvesting operations (Goodbody, Coops, Tompalski et al. 2017). The use of UAV-based DAP has also been evaluated in relation to tree detection for characterizing coniferous stands (Bonnet, Lisein, and Lejeune 2017), palm plantations (Sperlich et al. 2014; Kattenborn et al. 2014), and open mixed conifer forest (Mohan et al. 2017). However, to the best of our knowledge, no studies have yet compared the rate of detection of ITCs from SfM- and ALS-derived CHM in high-density *Eucalyptus* spp. plantations, characterized by complex terrain. Some questions regarding the processing of UAV-derived imagery for use in different types of forest have been highlighted by different authors (Dandois, Olano, and Ellis 2015; Bonnet, Lisein, and Lejeune 2017). The forest canopy surface is a complex layer, which is difficult to model by means of a digital surface model (DSM) or orthophoto mosaic (Lisein et al. 2013; Bonnet, Lisein, and Lejeune 2017). Moreover, knowledge about data acquisition and processing optimization and their implications for estimating forest inventory variables in different types of forest remains limited (Thiel and Schmullius 2017; Bonnet, Lisein, and Lejeune 2017).

In this study, we compared ALS- and UAV(SfM)-derived point clouds in the context of measuring a very dense Eucalyptus plantation in northern Portugal. This represents an environment that has not been evaluated previously and that represents certain challenges for both ALS- and UAV(SfM)-derived data due to the dense canopy cover (CC) and steep rugged terrain.

2. Materials and methods

2.1. *Study area*

The study area is located in the municipality of Valongo in the district of Porto, Portugal (Figure 1) (41.213° N, −8.496° W). It comprises a 7 years old plantation of *Eucalyptus* spp. clonal material (G74), covering an area of 26 ha. Tree spacing was 3.70 × 2.50 m, resulting in a density of 9.25 trees per m^2. The elevation of the area varies from 163 to 294 m above the WGS84 reference ellipsoid. The terrain is topographically complex, with steep slopes (mean slope 24.22%) and an elevation range up to 131 m. The mean annual rainfall is 1568 mm, with 42.1% of precipitation occurring between November and January. The mean annual temperature is 14.2°C, ranging from 8.6°C in the coldest months (December–February) to 20.1°C in the warmest months (July–September). The study site is characterized by evenly planted trees of superior genetic material and with a low mortality rate.

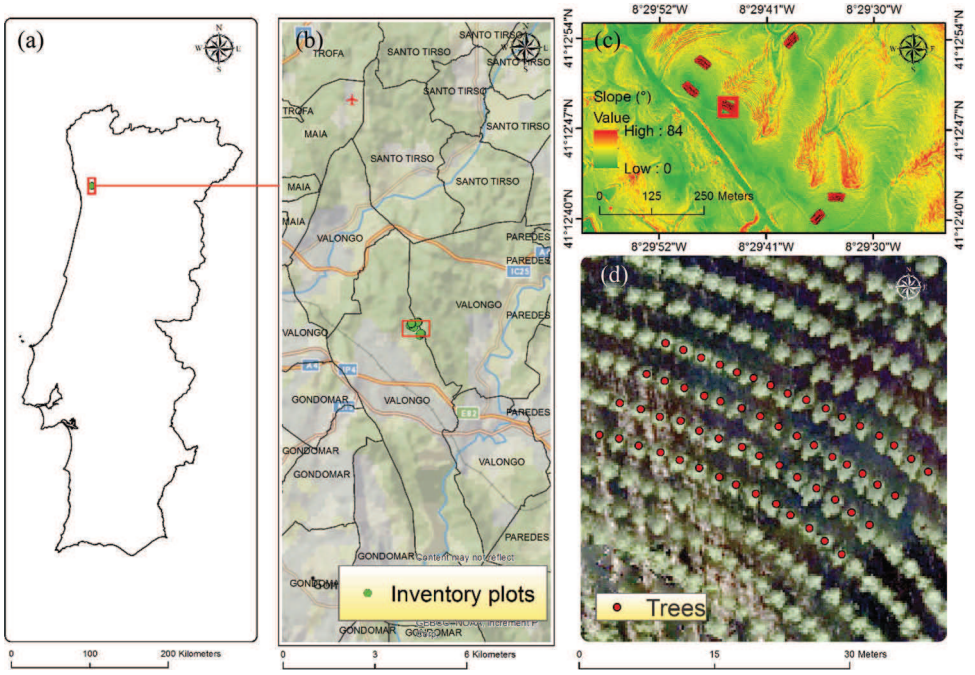

Figure 1. (a) Location of study area (Portugal), (b) location of Valongo (Porto, Portugal), (c) location of test area, and (d) location and design of one inventory plot.

2.2. *Field data*

The field data were collected in the winter of 2016 from 6 square plots each of approximately 400 m^2 (Table 1). The height of each tree (*h*, m) within the plots was measured with a Haglof Vertex IV hypsometer equipped with a T3 transponder. The diameter at breast height (1.30 m above the ground, *d*) was measured with a steel diameter measuring tape. Terrestrial Laser Scanning (TLS) measurements were made between 14 November and 16 November 2016, just before the traditional field inventory, and a stem map (i.e. location and identity code for each tree) was created. The trees were manually detected and labelled in the plots at this time. All the trees in the plots were subsequently used as reference trees for validating the tree detection process. Field plots were remeasured using the same methods in September 2017.

Table 1. Summary statistics describing the field plots.

					d				*h*			
Plot	*N*	Orientation	Mean slope (%)	CC (%)	mean	min	max	SD	Mean	min	max	SD
1	53	NE	24.2	57.5	13.2	10.4	17.0	1.1	19.4	15.4	21.6	1.1
2	65	SW	10.9	57.9	12.9	5.3	17.3	2.2	18.8	9.9	22.8	2.0
3	59	NE	15.0	51.8	13.4	7.4	16.0	1.5	18.6	13.5	20.1	1.2
4	49	NW	13.2	50.9	13.8	11.0	16.5	1.2	18.8	16.2	21.4	1.2
5	46	N	21.7	52.5	13.7	8.0	17.3	1.9	18.3	14.8	20.9	1.4
6	53	NW	20.4	45.0	13.8	6.0	16.8	2.1	17.6	12.4	19.8	1.4

N: Number of stems in the plot; *d*: diameter at breast height (1.3 m above ground, cm); *h*: measured tree height (m); min: minimum value; max: maximum value; SD: standard deviation; mean slope: per cent slope (%); CC: canopy cover (percentage of first returns above 5.00/total first returns) derived from ALS data (%).

In order to obtain very accurate positions of the trees, topographic surveys were conducted to determine the position of the centre of each tree within the plots. A Trimble® TSC3 GPS controller with Trimble® R8s Integrate GNSS System Antenna (Trimble, Sunnyvale, CA, USA) (dual-frequency real-time kinematic [RTK] receiver) was used to obtain the coordinates of a densified geodetic network for the study area by applying real-time kinematics. Based on the network established with the GPS, a topographic survey of the plots was conducted using a Trimble® M3 Robotic Total Station (Trimble, Sunnyvale, CA, USA). Observations on the position of each tree within the plot were made during the survey.

2.3. *ALS collection*

The airborne surveys were conducted on 17 December 2016 to cover an area of 100 ha. For this purpose, a Leica ALS80-HP laser scanner operating at pulse rate of 704 kHz, field of view of 6.5° (±3.25°), and scan rate of 73.5 Hz was mounted on a Cessna aeroplane that flew the area at an approximately flight altitude of 2750 m.a.s.l and an average speed of 250 km h^{-1}. The overlap between sweeps was 30%, and an average laser pulse density of 43.33 pulses m^{-2} was obtained.

2.4. *UAV data collection under cloudy conditions and non-optimal atmospheric conditions (SfM_1)*

The airborne surveys were conducted on 6 November 2016. Atmospheric conditions during the flight (from 12.30 a.m. to 13.07 p.m.) were characterized by moderate winds, partly cloudy weather and low illumination (winter conditions). An RGB SONY ILCE-5000 (20.1 MP) camera (Sony Co., Tokyo, Japan) was mounted, with nadir view, on a custom built fixed wing-UAV. The camera, equipped with a 5456 × 3632 pixel detector, captured images at ISO 200, shutter speed of 1/2500 s, and 16 mm focal length. A flight planning and monitoring software (Mission Planner, http://ardupilot.org/planner/) was used to determine the main flight parameters. Photographic side overlap was controlled by preprograming the automated UAV grid mission flight plan based on a designated flight altitude above the launch location and by the spacing between parallel flight tracks, respectively (Figure 2(a)). In total, 672 RGB images were acquired at a consistent altitude of 120 m (take-off at high point altitude in the study area) and the flight line spacing was 35 m. The total area covered was 117.26 ha, with an average Ground Sampling Distance (GSD) of 4.64 cm. The flight plan was designed to ensure a percentage of along (70%) – and across (70%) – track overlap between collected images. Moreover, one flight was needed to cover the whole area (one block).

2.5. *UAV data collection under clear lighting and optimal atmospheric conditions (SfM_2)*

The airborne surveys were conducted on 6 September 2017. Atmospheric conditions were characterized by calm winds, clear lighting atmospheric conditions at the flight time (between 11.30 a.m. and 12.15 p.m.) to minimize the effect of shadowing. An RGB S.O.D.A. 10.2 (20 MP) camera (senseFly Co, Cheseaux-Lausanne, Switzerland) was mounted, with nadir view, on a fixed-wing UAV (SenseFly eBee). The camera, equipped with a

12.75 × 8.5 mm sensor and 5472 × 3648 pixel detector, was used in manual mode, and exposure settings (ISO 150 and shutter speed of 1/1000 s) were set before each take-off according to the light conditions. This provided ~6 cm pixel^{-1} resolution for a variable altitude above ground level, which is especially useful in areas of diverse elevation range such as mountainous regions. eMotion V. 3.2.4 flight planning and monitoring software was used to determine the main flight parameters. The flight plan covered the entire study area with a longitudinal and lateral overlaps of 85% in both cases. The flight line spacing was 25 m (Figure 2(b)). In total, 744 images were used to generate orthomosaics and DSMs by the SfM image reconstruction process. Two-block flights were required to capture the entire forest study area (the orthomosaic covered an area 103.70 ha with average GSD of 5.95 cm). In total, 12 flight tests were required to achieve satisfactory results for comparison with ALS-derived point clouds. The airborne surveys were hampered by even moderate winds. Great effort was made to operate close to solar noon; large shadows projected by the trees were visible during most of the survey. Moreover, two subflights were needed to cover the whole area (two blocks) due to limited battery power.

2.6. *3D model generation*

The absolute orientation of the aerial photographs was determined using aerotriangulation techniques implemented in pix4D 3.3.29 (pix4D®, Ecublens, Switzerland). A set of 10 ground control points (GCPs) were measured in the field with topographic methods in order to georeference the SfM mosaics to a projected coordinate system for both data sets (Table 2). A pole equipped with a Trimble TSC3 controller and a Trimble R8s GNSS antenna (RTK precision 8 mm + 1 ppm horizontal/15 mm + 0.5 ppm vertical) was used to capture the ground control photogrammetric targets. The GCPs markers comprised a set of 1 × 1 m cross-shaped white painted timber planks with some black and white 50 × 50 cm painted checkerboards. For reliable accuracy of GPS measurement, all GCPs were located in open areas with no CC. At each point, GPS signals were logged in RTK–GNSS mode. The recordings were processed with real-time correction data retrieved from the fixed base station in Gaia (Porto) (latitude: 41° 06′

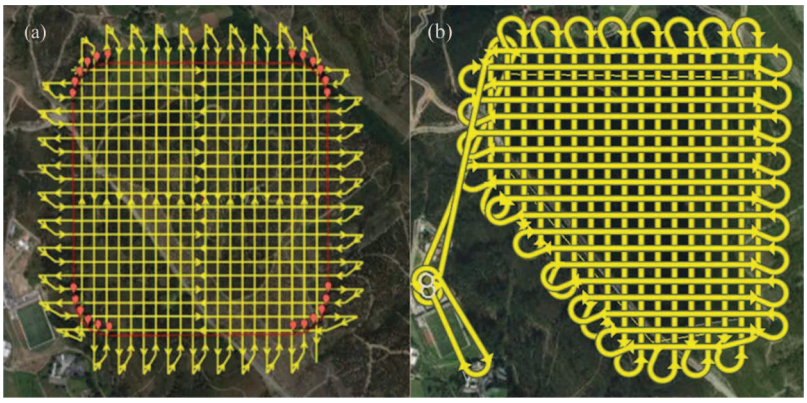

Figure 2. Flight designs (a) fixed-wing UAV data collection (SfM_1) at fixed altitude and non-optimal atmospheric conditions and (b) Fixed-wing UAV data collection (SfM_2) at variable altitude and under optimal weather conditions. Yellow lines represent the flight path.

Table 2. Summary statistics of the UAV-based DAP collections.

Data set	No. of GCPs	Density (points m^{-2})	$RMSE_X$ (m)	$RMSE_Y$ (m)	$RMSE_Z$ (m)
SfM_1	10	48.85	0.004	0.010	0.0557
SfM_2	10	96.63	0.037	0.032	0.1554

SfM_1: UAV-based DAP collection in partly cloudy atmospheric condition and fixed altitude; SfM_2: UAV-based DAP under clear lighting and optimal atmospheric conditions and variable altitude; GCPs: ground control points; $RMSE_X$, $RMSE_Y$, and $RMSE_Z$ are the root mean square error in the direction of the three spatial coordinates (*X*, *Y*, and *Z*), reflecting the planimetric and altimetric accuracy in the GCPs.

21.67048″ N, longitude: 8° 35′ 20.73434″ W, and ellipsoidal elevation: 287.63 m above the WGS84 reference ellipsoid). Image mosaics and photogrammetric point clouds (DSMs) (Figure 3) were computed using SfM techniques, as implemented in Pix4D 3.3.29. The matching parameters for point cloud densification were set as follows: multiscale, image scale = 1/2 (half image size), and point density = 'optimal.' The minimum number of matched images was also set to 3. By way of example, the time computation required to produce a georeferenced point cloud from SfM_2 project, using pix4D 3.3.29 installed on a dual Intel (R) Core (TM) i7-5820K CPU @3.30 GHz workstation with 64 GB of RAM, was approximately 9 h and 53 min for point cloud densification, 39 min and 08 s for DSM generation, 2 h and 17 min for the orthomosaic, and 08 min and 01 s for the DEM generation.

2.7. *Point cloud processing*

Preprocessing of ALS and SfM point clouds (Figures 4(a) and (b)) was performed using FUSION/LDV 3.60 software (McGaughey 2016) and LasTools (Isenburg 2016). Ground

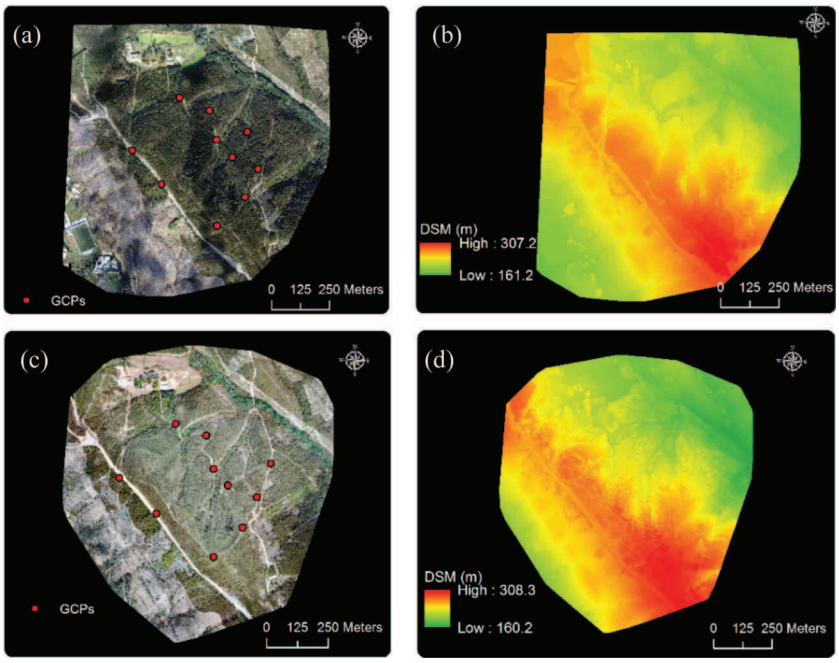

Figure 3. UAV-derived orthomosaic using SfM_1 (a) and SfM_2 (c) data collections. UAV-derived DSMs generated from Pix4d using SfM_1 (b) and SfM_2 (d) data collections.

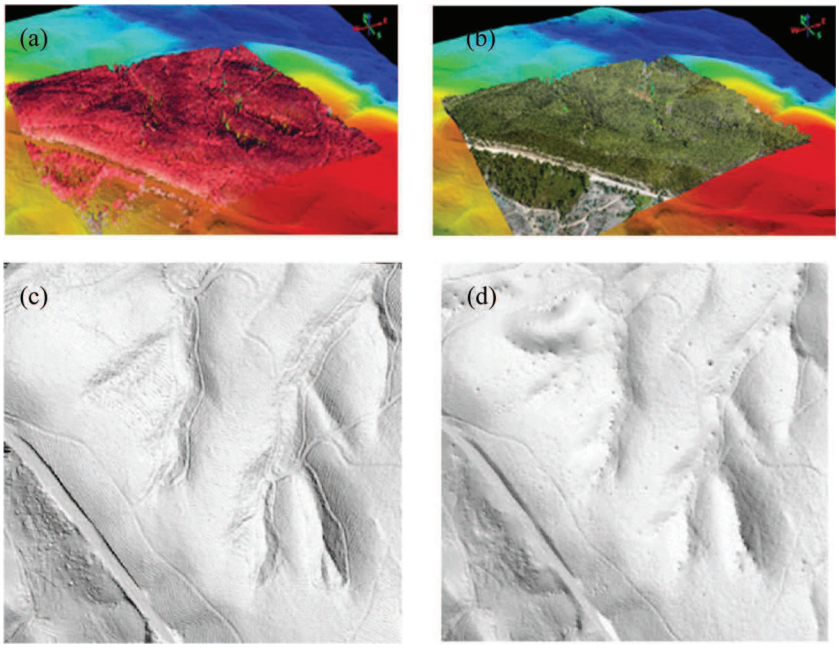

Figure 4. (a) Digital surface model (DSM) derived by ALS, (b) digital surface model (DSM) derived by SfM_2, (c) DEM-derived by ALS (LasTools), and (d) DEM derived by SfM_2 (Pix4d 3.3.29).

returns from the ALS point cloud were isolated to generate the DEM_{ALS} and to normalize the point cloud. At landscape level, ground points were classified using a Progressive triangulated irregular network densification algorithm implemented in *lasground* (settings: -nature, -extrafine, spike: 1 m, and offset: 0.05 m), and a DEM of 0.20 m cell size was interpolated using the *GridSurfaceCreate* tool in FUSION/LDV 3.60 (Figure 4(c)). The DEM_{SfM2} of 30 cm $pixel^{-1}$ was generated using the photogrammetric software Pix4d 3.3.29 from the SfM_2 data collection (Figure 4(d)). A DEM was not generated from the SfM_1 data collection as the SfM_1-derived point clouds were incomplete and only covered the upper parts of the canopy (Figure 5), whereas SfM_2-derived point cloud was complete and penetrated the canopy to some degree, reaching the ground in most cases under clear lighting and optimal atmospheric conditions. At plot level, the *PolyClipData* tool in FUSION/LDV 3.60 was used to extract a subset of the ALS and SfM points clouds within each buffer plot (Figure 5). The ALS-derived CC (%) was then estimated for each plot by using *Cover* tool in FUSION/LDV 3.60, which computes CC as the ratio between the number of first pulses returned from the upper layer of tree crown (a threshold height of 5 m) and all first returns (throughout the canopy to ground profile) (Table 1).

2.8. *CHM generation*

CanopyModel tool, also implemented in FUSION/LDV, was used to compute a set of four CHMs with 0.20 m of spatial resolution for the study site (Table 3, Figure 6). CHM_I was obtained as the difference between the DSM_{ALS} and DEM_{ALS} (Figure 6(a)), while CHM_{II}, CHM_{III}, and CHM_{IV} were generated using two approaches: in the first two, the DEM_{ALS} was

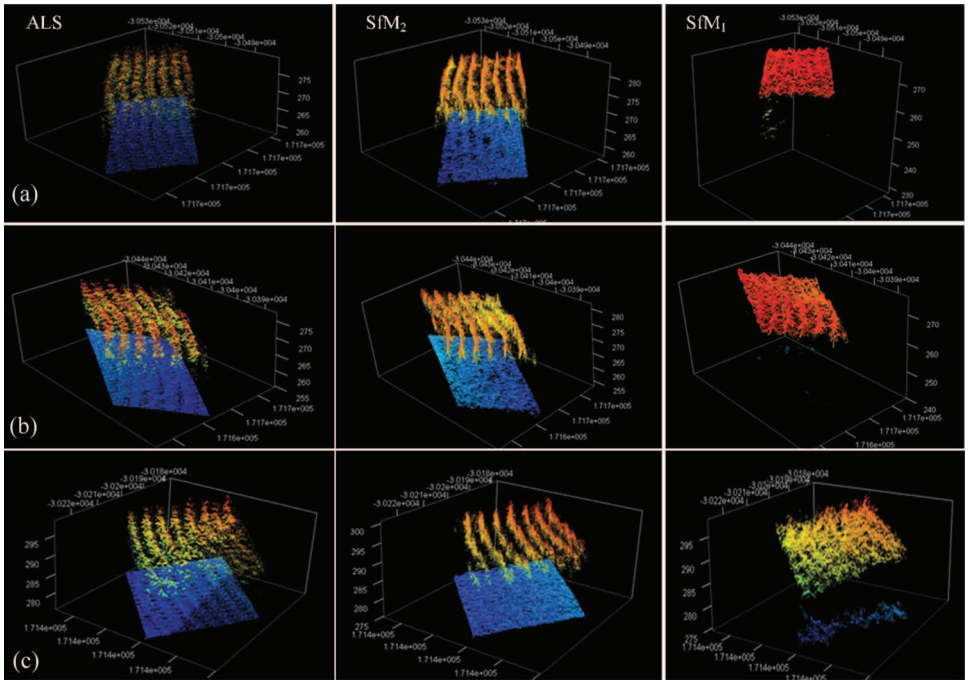

Figure 5. Subsets of ALS- and SfM-derived point clouds for plot 2 (a), plot 3 (b), and plot 4 (c).

Table 3. Nomenclature of the CHMs resulting from the subtraction of DEMs to the DSMs for the four point cloud acquisitions.

DSM point-clouds	DEM	CHM
DSM_{ALS}	DEM_{ALS}	CHM_{I}
DSM_{SfM1}	DEM_{ALS}	CHM_{II}
DSM_{SfM2}	DEM_{ALS}	CHM_{III}
DSM_{SfM2}	DEM_{SfM2}	CHM_{IV}

subtracted from the DSM_{SfM1} and DSM_{SfM2} point clouds, respectively (CHM_{II} and CHM_{III}, respectively, Figures 6(b) and (c)), and in the third, the DEM_{SfM2} was subtracted from the DSM_{SfM2} (CHM_{IV}, Figure 6(d)). A mean smooth filter with fixed smoothing window sizes of 3×3 and 5×5 m was used for the smoothing process by applying the *CanopyModel* tool.

2.9. *ITC delineation*

The accuracy of tree detection is known to be sensitive to the algorithm settings and can vary depending on the forest type and structure. We therefore decided to use a simple but widely used algorithm: local maxima detection with a fixed size window. The *CanopyMaxima* tool of FUSION/LDV 3.60 software (McGaughey 2016) implements the algorithm developed by Popescu, Wynne, and Scrivani (2004). The smoothed CHMs, denoted CHM_{I}, CHM_{II}, CHM_{III}, and CHM_{IV}, were used as inputs. The window size is usually derived from an empirical relationship between tree height and crown diameter (Popescu, Wynne, and Nelson 2003). However, such a relationship was not used here

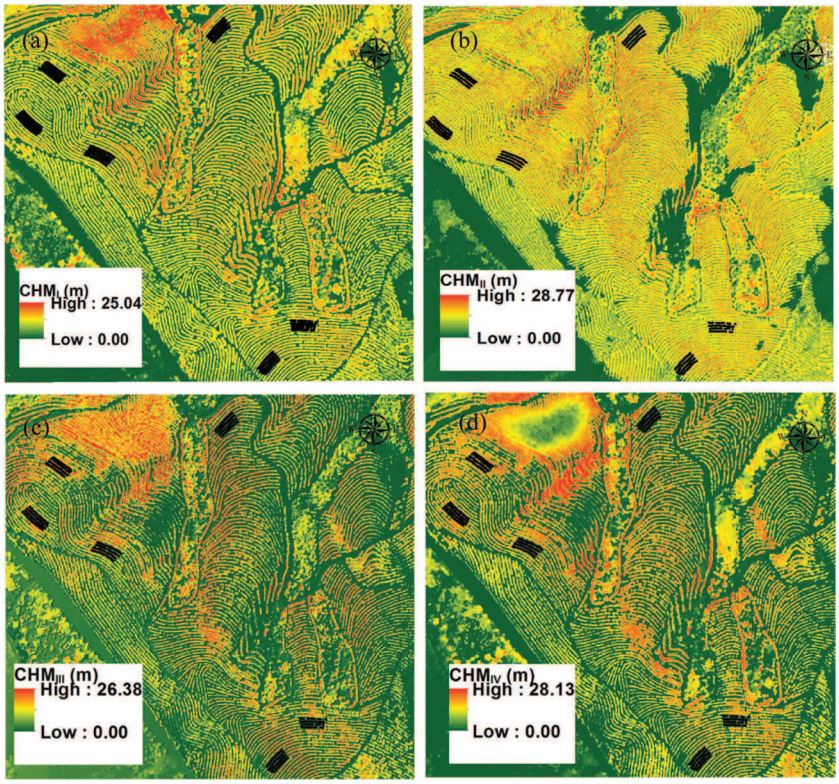

Figure 6. Corresponding rasters for CHM_I (a), CHM_{II} (b), CHM_{III} (c), and CHM_{IV} (d).

because of the lack field measurements of crown diameter. Equation (1) was used instead to determine the *CanopyMaxima* tool window size from the height of the surface at the centre of the window.

$$W = A + B \times h + C \times h^2 + D \times h^3 \quad (1)$$

where W (width) is the window size, A, B, C, and D are polynomial coefficients, and h is the corresponding CHM height.

A fixed window size (FWS) was tested by applying constants of 0.5, 1.0, and 1.5 for the intercept of the equation and 0 for h for the 8 different CHMs (I, II, III, and IV, which were previously smoothed with kernel sizes of 3 × 3 and 5 × 5 pixels). The other *CanopyMaxima* parameters were set as follows: ALS: res = 1.0, mult = 1.0, SfM-UAV: res = 0.15, mult = 1.0. The minimum tree height threshold was 5 m.

The accuracy resulting from using CHM_I, CHM_{II}, CHM_{III}, or CHM_{IV} was estimated via five different measures: percentage of trees detected (Equation (2)), relative omission and commission errors (Equations (3) and (4)), root mean square error (RMSE), and bias of the predicted height of linked trees (Equations (5) and (6)). A tree was considered correctly detected when the tree position was located within the 1.2 m buffer radius of the reference tree position (Table 5). When more than one candidate tree fell within the buffer, the candidate closest to the top of the field-observed tree was linked to the field-measured tree. In the case of individual tree height analysis, the heights of the linked pairs

were compared in order to remove gross linking errors (Vauhkonen et al. 2011). A plotwise of ALS and SfM-linked tree heights was constructed for the best combinations from the eight data sets, CHM_{I}, CHM_{II}, CHM_{III}, and CHM_{IV}, and those tree-candidate links for which the height difference was greater than 5 m were removed (González-Ferreiro et al. 2013).

$$\text{Detected trees} = \frac{N_{\text{detected}}}{N_{\text{rel}}} \tag{2}$$

$$\text{Error of omission} = \frac{N_{\text{missed}}}{N_{\text{rel}}} \tag{3}$$

$$\text{Error of commission} = \frac{N_{\text{extra}}}{N_{\text{rel}}} \tag{4}$$

where N_{detected} is the number of trees found, N_{missed} is the number of undetected trees, N_{extra} is the number of unmatched tree candidates, and N_{rel} is the number of reference trees.

$$\text{RMSE} = \sqrt{\frac{\sum_{i=1}^{n} (y_i - \hat{y}_i)^2}{n}} \tag{5}$$

$$\text{Bias} = \frac{\sum_{i=1}^{n} (\hat{y}_i - y_i)}{n} \tag{6}$$

where n is the number of trees, y_i is the field measured tree height i, and $\hat{y}_i$ is the estimated value of CHM-derived tree height i.

3. Results

3.1. *Comparison of SfM- and ALS-derived DEMs*

Direct comparison of the GPS-surveyed GCPs and the two DEM products resulted in a mean overestimation of 0.18 m (SD = 0.30 m) for the DEM_{SfM2}, while the DEM_{ALS} exhibited a mean overestimation of 0.28 m (SD = 0.16 m). The GPS-based comparisons for the DEM products are summarized in Table 4.

Subtracting the DEM_{ALS} from the DEM_{SfM2} produced a spatial evaluation of the differences between the two DEM products (Figure 7(a)). Over the entire study area, the DEM_{SfM2} tended to be within ±1 to ±2.0 m of the DEM_{ALS}. DEM_{SfM2}-negative prediction indicates that the SfM surface elevation is below the ALS surface elevation (areas shown in green in Figure 7(a)). Negative differences tend to occur in steeply sloping areas, on the lowest sides of the valley

Table 4. Summary of GPS-surveyed plot ground control points and DEM product comparisons at landscape level.

Difference between	ZGPS − $ZDEM_{SfM2}$	ZGPS − $ZDEM_{ALS}$	$ZDEM_{SfM2}$ − $ZDEM_{ALS}$
Mean (m)	0.18	0.28	1.14
Minimum (m)	−0.04	−0.14	−6.17
Maximum (m)	0.64	0.47	18.91
SD (m)	0.30	0.16	1.93

SD: Standard deviation of the differences.

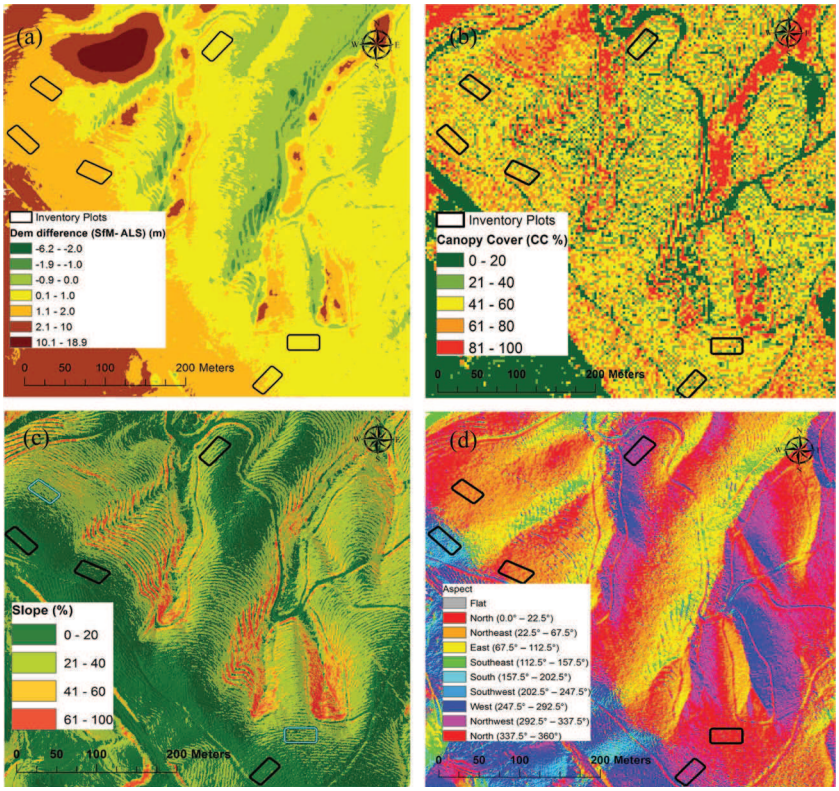

Figure 7. (a) Spatial distribution of elevation differences between the DEM_{SfM} and DEM_{ALS} (m). Areas where the DEM_{SfM} was modelled below the DEM_{ALS} are shown in green, and areas above the DEM_{ALS} are shown in orange and brown and yellow; (b) raster grid of 3 m pixel size representing canopy cover (CC, %) estimated from ALS data (CC was calculated as percentage of first returns above 3.00/total all first returns); (c) slope (%) throughout the study area (location of plots 1 and 5 with higher slope highlighted in blue); and (d) view of the study area showing the location and orientation of the plots.

with a southeast orientation. The DEM_{SfM}-positive prediction indicates that the SfM surface elevation is higher than the modelled ALS surface elevation. These areas, displayed in yellow, orange, and brown in Figure 7(a), tend to occur in areas of dense CC and where the lack of ground points results in larger interpolation distances. Very large differences in DEM_{SfM2} (e.g. > +2.0 m) occur in the northern parts of the study area (Figure 7(a)). Few 3D non-tree canopy points were generated within this densely vegetated area (>60% of CC, Figure 7(b)), and none were classified as ground points. Overall, the lack of ground points resulted in larger interpolation distances for this area. On average, the interpolated DEM_{SfM} surface was 1.14 m (SD = 1.93 m) higher than the interpolated DEM_{ALS} surface.

3.2. *ITC delineation*

Use of a FWS of 1 × 1 m in the *CanopyMaxima* tool proved optimal for individual tree detection in both technologies. We also verified that increasing the FWS led to decreased accuracy. The

Table 5. Individual tree detection in plots.

		Found tress		Omission error		Commission error	
Model	Plot	3 × 3	5 × 5	3 × 3	5 × 5	3 × 3	5 × 5
CHM_I	1	50 (90.6%)	50 (90.6%)	3 (5.7%)	5 (0.1%)	8 (11.3%)	0 (9.4%)
	2	65 (96.9%)	60 (92.3%)	0 (0.0%)	5 (0.1%)	10 (12.3%)	3 (7.7%)
	3	59 (100%)	59 (100%)	0 (0.0%)	0 (0.0%)	3 (5.1%)	0 (0.0%)
	4	49 (100%)	49 (100%)	0 (0.0%)	0 (0.0%)	4 (8.2%)	0 (0.0%)
	5	46 (100%)	46 (100%)	0 (0.0%)	0 (0.0%)	6 (13%)	0 (0.0%)
	6	52 (92.5%)	52 (92.5%)	1 (1.9%)	4 (0.1%)	20 (32.1%)	5 (7.6%)
	Total	**321 (96.7%)**	**311 (95.9%)**	**4 (1.3%)**	**14 (4.1%)**	**51 (13.7%)**	**8 (2.3%)**
CHM_{II}	1	20 (35.9%)	20 (35.0%)	33 (62.3%)	33 (62.3%)	20 (35.9%)	20 (37.7%)
	2	49 (75.4%)	44 (67.7%)	16 (24.6%)	21 (32.3%)	1 (1.5%)	0 (0.0%)
	3	34 (57.6%)	34 (57.6%)	25 (42.4%)	25 (42.4%)	0 (0.0%)	0 (0.0%)
	4	28 (57.1%)	24 (49.0%)	21 (42.9%)	25 (51.0%)	2 (4.1%)	1 (2.0%)
	5	25 (54.4%)	21 (45.7%)	21 (45.7%)	25 (54.4%)	0 (0.0%)	0 (0.0%)
	6	40 (75.5%)	40 (75.5%)	13 (24.5%)	13 (24.5%)	1 (1.9%)	1 (1.9%)
	Total	**196 (59.3%)**	**183 (49.2%)**	**129 (40.4%)**	**142 (44.5%)**	**24 (7.2%)**	**22 (6.9%)**
CHM_{III}	1	35 (66.0%)	32 (60.4%)	17 (34.0%)	21 (39.6%)	2 (3.8%)	1 (1.9%)
	2	54 (83.1%)	52 (80.0%)	11 (16.9%)	13 (20.0%)	9 (13.9%)	7 (10.8%)
	3	45 (76.3%)	41 (69.5%)	14 (23.7%)	18 (30.5%)	0 (0.0%)	0 (0.0%)
	4	44 (89.8%)	29 (63.0%)	5 (10.2%)	17 (14.3%)	5 (10.2%)	0 (0.0%)
	5	32 (69.6%)	42 (85.7%)	14 (30.4%)	7 (37.0%)	0 (0.0%)	5 (10.0%)
	6	48 (90.6%)	48 (90.6%)	5 (9.4%)	5 (9.4%)	6 (11.3%)	5 (9.4%)
	Total	**259 (79.6%)**	**244 (74.9%)**	**66 (20.8%)**	**81 (25.1%)**	**22 (6.5%)**	**18 (5.4%)**
CHM_{IV}	1	37 (69.8%)	33 (62.3%)	16 (30.2%)	20 (37.7%)	4 (7.6%)	2 (3.8%)
	2	51 (78.5%)	49 (75.4%)	14 (21.5%)	16 (24.6%)	9 (13.9%)	11 (16.9%)
	3	42 (85.7%)	41 (69.5%)	7 (14.3%)	18 (30.5%)	5 (10.2%)	1 (1.7%)
	4	42 (71.2%)	45 (91.8%)	17 (28.8%)	4 (8.2%)	3 (5.1%)	4 (8.2%)
	5	30 (65.2%)	30 (65.2%)	16 (34.8%)	16 (34.8%)	0 (0.0%)	0 (0.0%)
	6	46 (86.8%)	48 (90.6%)	7 (13.2%)	5 (9.4%)	8 (15.1%)	8 (15.1%)
	Total	**248 (76.2%)**	**246 (75.8%)**	**77 (23.8%)**	**79 (24.2%)**	**29 (8.6%)**	**26 (7.6%)**

The results highlighted in bold type represent the best combination for the eight data sets, CHM_I, CHM_{II}, CHM_{III}, and CHM_{IV} with kernel sizes of 3 × 3 and 5 × 5 pixels, which were determined by comparing the number of trees detected with the field-observed number of trees. In brackets, the percentage of trees/number of reference trees in field plots.

accuracy of detection of individual trees using Mean Filter with kernels of 5 × 5 and 3 × 3 pixels is shown in Table 5. The best detection rate was obtained with CHM_I, whereas CHM_{II} option yielded the lowest detection rate. The omission error followed the same pattern. Smooth combinations were found to be a determining factor in the accuracy of ITC by ALS and SfM. The 3 × 3 kernel was also found to be favourable to the success of ITC delineation. However, in the case of ALS (CHM_I), the commission error was higher with this filter. The 5 × 5 kernel led to overestimation of tree tops. Finally, we tested the accuracy for the best combination, i.e. the 3 × 3 kernel for SfM (CHM_{II}, CHM_{III}, and CHM_{IV}) and the 5 × 5 kernel in the case of ALS (CHM_I).

In terms of the total number of tree candidates produced (i.e. the number of trees found plus the commission error), CHM_{II} and CHM_I represented the study extremes. In the case of CHMs obtained using SfM data (CHM_{II}, CHM_{III}, and CHM_{IV}), the least accurate results for the ITC delineation were mainly obtained in the most steeply sloping test subplots 1 and 5 (i.e. in plot 1, see Figure 8(a)) and higher CC. Although the mean slope of plot 6 was similar to those of plots 1 and 5, the detection rate achieved was higher due to lower CC (CC = 45%) (Figure 8(b)). On average, 95.9% of trees were detected correctly using the CHM_I, with omission and commission errors limited to 4.1% and 2.3%, respectively. In contrast, the algorithm detected only 79.6% in CHM_{III} and the associated omission and commission errors were 20.8% and 6.5%, respectively. In the case of CHM_{II} under non-optimal atmospheric conditions, local maximum algorithm detected only 59.3% of the trees, with omission and

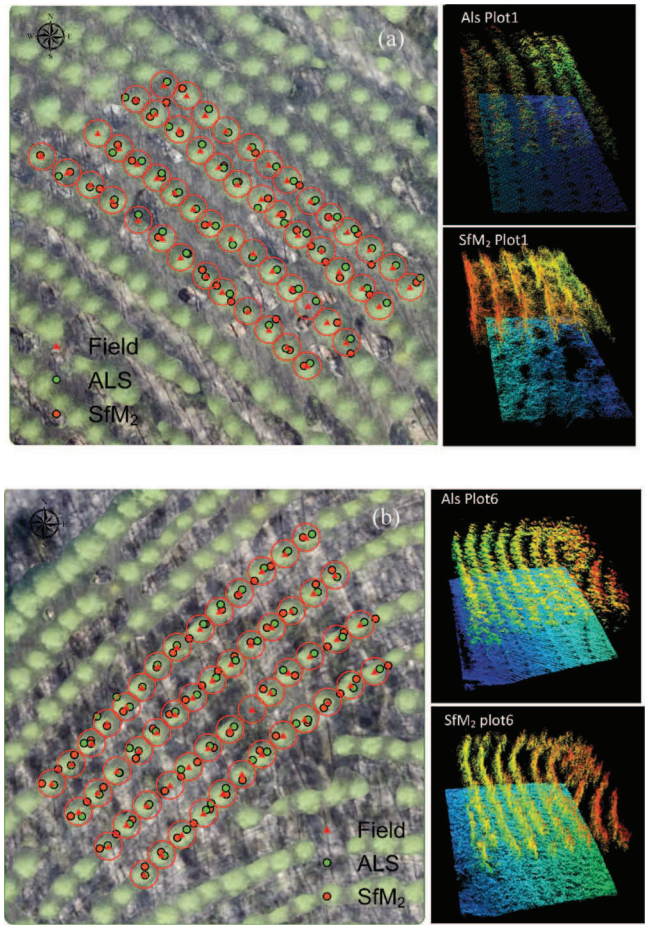

Figure 8. Results of individual tree detection with the best combinations of CHM_I (ALS) and CHM_{III} (SfM_2): plot 1 (a) and plot 6 (b).

commission errors of, respectively, 40.4% and 7.2%. Finally, the rate of detection was slightly lower (less than 3.4% in terms of trees found) with CHM_{IV} than with CHM_{III}.

3.3. *Individual tree height analysis*

We validated tree height by comparing the height of field-measured trees and ALS- and SfM-linked trees. A total of 300, 183, 251, and 237 previously matched trees of heights from, respectively, CHM_I, CHM_{II}, CHM_{III}, and CHM_{IV} were used for this purpose. The RMSE values were 2.80, 2.42, 1.82, and 2.84 m and the bias values were −2.59, −2.19, −1.47, and −2.67 m, respectively, for the four data sets. Field measurements of height were plotted against the corresponding remotely derived tree heights over the whole set of plots (Figure 9). The *r* (correlation coefficient) values were 0.66, 0.61, 0.67, and 0.69, respectively.

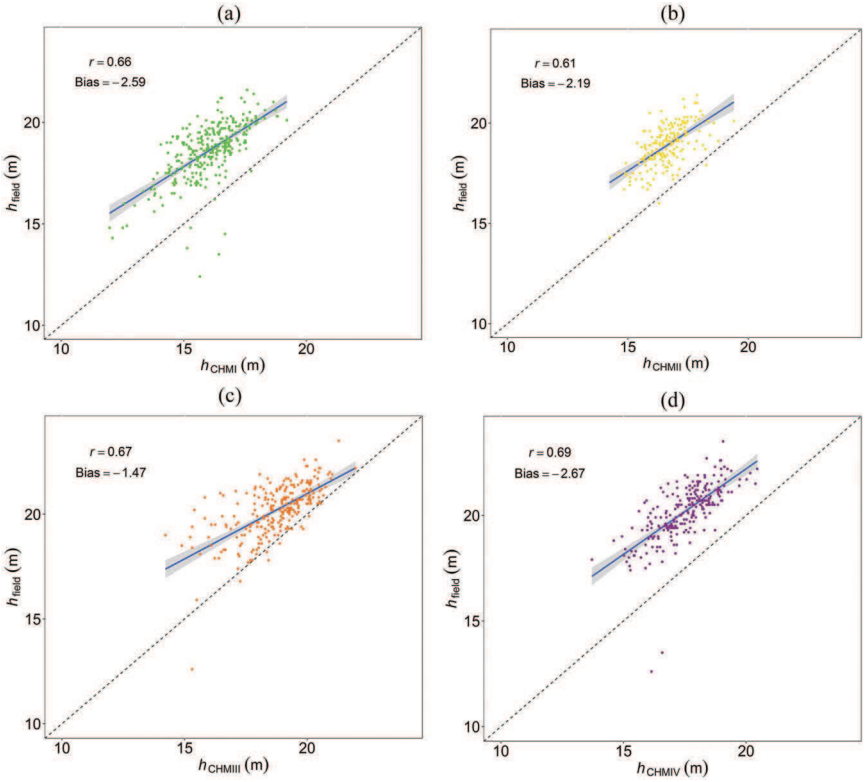

Figure 9. Scatter plots of (a) field-measured tree height (*h*) against ALS-derived tree height using CHM_I, (b) field-measured tree height (*h*) against SfM-derived height using CHM_{II}, (c) field-measured tree height (*h*) against SfM-derived height using CHM_{III}, and (d) field-measured tree height (*h*) against SfM-derived height using CHM_{IV}.

4. Discussion

The results for the study area demonstrate that SfM-derived point clouds can be used to generate accurate DEMs over vegetated surfaces, although some difficulties were experienced in closed canopy and steep slope areas. We also observed that the DEM_{SfM2} accuracy derived from pix4d was influenced by the orientation. The DEM_{SfM2} tended to be more accurate in steep areas with southeast orientation, due to the lower density of leaves in the crowns and lower presence of shrub cover. However, the opposite effect was observed in north-facing areas. DEM_{ALS} outperformed aerial imaging techniques in mapping terrain as DEM_{SfM2} tended to overestimate height comparing with DEM_{ALS}, particularly in steeply sloping areas of dense vegetation cover, as also reported Jensen and Mathews (2016). In case of major differences in DEM_{SfM} (e.g. >±2.0 m), in which poor performance of the SfM ground filtering algorithm is expected, manual editing of ground *versus* non-ground points in these areas might be advisable.

In terms of the detection rate, the most accurate results from ALS- and SfM-derived point clouds were found by applying a *Mean Filter* algorithm with kernel sizes of 5 × 5 and 3 × 3 pixels, respectively. Similar results were reported by Silva et al. (2016) and Mohan

et al. (2017), for ALS- and SfM-derived point clouds, respectively. These authors found that 5 × 5 and 3 × 3 kernels eliminated spurious local maxima caused by the irregularity of tree crowns and tree branches and confirmed that the higher success rate of the 3 × 3 kernel can be attributed to denser canopy over the study sites. Nonetheless, the combinations of filter sizes can also be affected by forest types and tree size (Lindberg and Hollaus 2012; Mohan et al. 2017; Bonnet, Lisein, and Lejeune 2017). Depending on the intended use, there will always be a trade-off between commission and omission errors, and the overall efficiency of a particular window size can be viewed as a function of the object and resolution relationship, which can serve as an initial step towards the development of site-specific tree identification models (Wulder, Niemann, and Goodenough 2000).

In the case of ALS-derived data, tree detection results from this study are similar or slightly better than those obtained in other studies using higher ALS density data. In particular, our values were similar to those reported by Wack et al. (2003) for a low density *Eucalyptus* spp. plantation in Portugal (accuracy: 93%; ALS density: 5 pulses m^{-2}) and much better than those reported by Gonçalves-Seco et al. (2011) for the very dense *Eucalyptus globulus* stands in Galicia (Spain) and using low ALS point density (accuracy: 37.2%; ALS density: 4 pulses m^{-2}). Vauhkonen et al. (2011) tested six different algorithms from which four applied CHM for detecting single trees in varying forest conditions. The algorithms performed similarly and the differences between detection rates (from 45.2% to 100.7%) were more strongly affected by forest structure (e.g. tree density and clustering) than by the use of different algorithms. Omission errors (i.e. trees not detected, usually suppressed under dominant canopy layer) varied between 30.6% and 61.1%, whereas commission errors varied from 6.9% to 39.4%.

Evaluation of the results should take into account the difference in the costs of the SfM- and ALS-based data acquisition. In the case of the SfM-derived point clouds, our findings demonstrated that UAV images and CHM can be used efficiently to identify individual trees particularly in the context of *Eucalyptus* spp. stands on complex terrain. The values obtained in the present study were slightly lower, in terms of percentage detection rate, than those reported by Mohan et al. (2017) for an open canopy mixed forest in USA (overall accuracy of 91.6%, and with omission and commission errors of 5.7% and 2.7%, respectively, using a rotatory-wing aircraft) and by Bonnet, Lisein, and Lejeune (2017) for conifer stands including *Picea abies* (L.) H. Karst. (89.2% true positives, 10.8% omission, and 7.8% false positives in autumn at a flight altitude of 200 m above ground level using rotatory-wing aircraft). Nevalainen et al. (2017) achieved results with 64–96% tree identification rates within a buffer search radius of 2 m. However, the estimated accuracy of tree detection cannot be evaluated, due to the lack of reference data for testing. Kattenborn et al. (2014) upgraded Sperlich's algorithm by geometrically classifying UAV-derived point clouds and detected individual palm trees with an overall mapping accuracy of 86.1% for 9.4 ha of the entire study area and 98.2% for dense palm stands. The uncertainty in the number of trees detected in this study may be affected by the canopy structure and topographic conditions. For example, Tanhuanpää et al. (2016) obtained an accurate detection rate (97%) in pine-dominated stands, using DAP-derived point clouds from different forest types. The local maxima-based method was successful for conifers and boreal forest in which the trees have pointed crowns, although further fine-tuning is probably needed to obtain successful results in forests with less identifiable crowns as our study confirmed in the case of *Eucalyptus* spp. plantations.

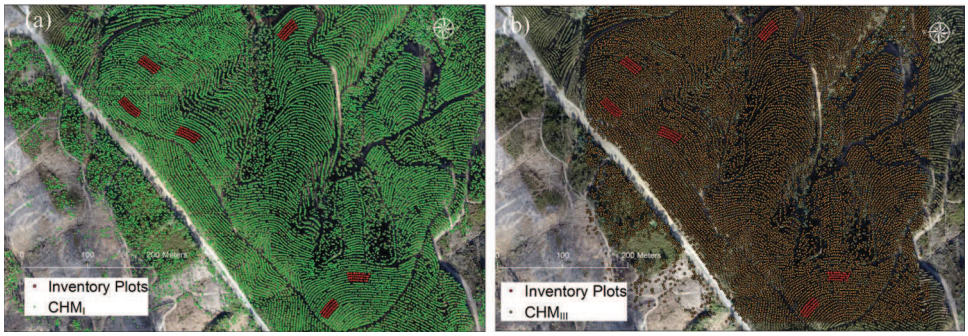

Figure 10. Individual tree detection at landscape level using CHM_I (a) and CHM_{III} (b).

In light of the study findings, we conclude that one of the key issues when using UAV-based DAP in detecting individual trees is the inconsistency of the detection rates between different plots and around the study area, especially in steep slopes where ALS performed better (Figure 9(a)). Among the methods tested, CHM_{ALS} seems to be the best model for detecting ITCs. Although the point cloud density of the SfM-derived CHMs was slightly higher, the ALS-derived CHMs captured the canopy variations better, probably because the images are strongly affected by variation in illumination and shadows in these dense CC and steep and rugged terrain. The rates of detection obtained confirmed that in more steeply sloping plots (see plots 1 and 5: Table 1, Figure 7(c)), the generation of point clouds was incomplete due to matching failures or occlusions (e.g. due to steep slopes or insufficient overlapping), and there were thus local inaccuracies in the 3D point cloud and CHM. Although the mean slope of plot 6 was similar to that of plot 1 (CC = 57.51%) and 5 (CC = 52.51%), the detection rate was higher probably because CC was lower (CC = 45%). The presence of shadows and other variations in the pictures may be problematical, especially when the photogrammetric processing products are used for classification (Baltsavias et al. 2008; Ke and Quackenbush 2011; Simic Milas et al. 2017). These classifications are usually based on the spectral response of objects with variations in the images leading to confusion of the objects identified (Laliberte et al. 2010; Ke and Quackenbush 2011). To prevent such variations, the flights for image collection should be performed during stable weather conditions, as observed by Näsi et al. (2015) and Guerra-Hernández et al. (2017) and with the smallest zenit solar angle possible (White et al. 2013; Dandois, Olano, and Ellis 2015). In mature forests, shadows are naturally created by the canopy structure (Puttonen, Litkey, and Hyyppä 2009; Wallace et al. 2016), and they are therefore more difficult to avoid.

Our findings are consistent with those of previous studies comparing ALS and SfM-generated point clouds and derived products to estimate individual tree height (Dandois and Ellis 2013; Jensen and Mathews 2016; Thiel and Schmullius 2017). The tree height was underestimated with all CHM methods, which is typical for both SfM- and ALS-based approaches (St-Onge et al. 2004; Suárez et al. 2005; Dandois and Ellis 2013; Jensen and Mathews 2016; Guerra-Hernández et al. 2017). Although similar, our results are slightly poorer in terms of *r* than those of prior studies, due to the characteristics of the type of forest (Gatziolis, Fried, and Monleon 2010; Gonçalves-Seco et al. 2011) and topographically complex

terrain in which data characteristics such as scan angle often cause inaccuracies in the DEMs that affect ALS-derived tree height (Raber et al. 2002; Estornell et al. 2011). These studies demonstrated the ability of ALS-based data sets to account for approximately 70–93% of field measured variability with prediction errors (typically as underestimates) of roughly 1–3 m (e.g. Næsset, Bollandsås, and Gobakken 2005; Gatziolis, Fried, and Monleon 2010; González-Ferreiro et al. 2013). *Eucalyptus* spp. trees do not usually have more than one apex in each crown. However, field tree height measurement and crown delineation remain difficult because (1) the crowns of trees are more spherical than the crowns of coniferous trees, (2) the crowns of neighbouring trees often overlap due to the high density of trees per unit area, and (3) the low density of leaves in the crowns (caused by repeated attacks by *Gonipterus scutellatus* Gyll.) and the small size of the crowns of mature trees prevent a considerable number of laser pulses from hitting the crown (thus hampering crown delineation). Our results confirmed that, at plot level, use of the SfM photogrammetric technique for interpolating the terrain surface below closed CC leads to overestimation of the ground elevation (Dandois and Ellis 2013; Jensen and Mathews 2016; Guerra-Hernández et al. 2017) and hence an underestimation of tree height. On the other hand, our results suggest that, at plot level, SfM-derived point cloud products perform as well as ALS data for estimating individual tree height, particularly in high-density *Eucalyptus* forests. However, our results confirmed that the use of UAV imagery to generate 3D point clouds over high CC landscapes and steep slopes must be considered with caution, especially above 60% of CC and 20% of slope.

The most accurate values in the present study were obtained during the summer, under fine weather conditions, with a high degree of overlap, variable flight altitude following the terrain elevation variation and minimum zenit solar angle possible. Although the results for both flights were not fully comparable, because of the use of different DAP sensors and UAV, the results of SfM_1 for data obtained under non-optimal atmospheric condition and fixed flight altitude demonstrated how seasonal differences in illumination and UAV-image-acquisition conditions may affect generation of the 3D DSM point cloud and consequently the detection rate.

5. Conclusion

A simplified framework for automated ITC delineation from UAV(DAP)-based and ALS-based point clouds is presented. The UAV-based DAP applications represent a pioneering approach for automatic ITC delineation in high-density Eucalyptus plantations and showed a similar efficiency to ALS solutions. However, atmospheric flight conditions and topographic complex terrain were limiting factors at landscape level. The proposed methodology is potentially a highly effective, affordable, and easy-to-use approach for ITC delineation and therefore for guiding mission flight planning, forest monitoring, and inventory management. This study also demonstrates that, at plot level, image-based point clouds are a potentially robust, low-cost alternative source of tree height estimation in this type of forest. However, at landscape level, ALS is superior because of its ability to penetrate canopy gaps and to record returns from the ground. A comprehensive examination of the effects of varying the conditions of UAV-SfM remote sensing on 3D point cloud traits and canopy metrics revealed also important insights into the effect of data quality and slope terrain in the ITC delineation process using with these

techniques. Our findings add information to the growing body of literature on the potential use of UAV-acquired data in forestry.

Acknowledgements

We gratefully acknowledge RAIZ and the Navigator Company for supplying the inventory databases and support the airborne surveys and TLS field work. We thank the Portuguese Science Foundation (SFRH/BD/52408/2013) for funding the research activities of Juan Guerra and the Galician Government and European Social Fund (Official Journal of Galicia – DOG No. 52, 17/03/2014 p. 11343, exp: POS-A/2013/049) for funding the postdoctoral research stays of Eduardo González-Ferreiro. This research was supported by SuFoRun project 'Models and decision SUpport tools for integrated FOrest policy development under global change and associated Risk and Uncertaint' funded by the European Union's H2020 research and innovation programme under the Marie Sklodowska Curie Grant Agreement No. 691149. We also acknowledge support from Terradrone Co. during the airborne survey. The research was carried out in the Centro de Estudos Florestais: a research unit funded by Fundação para a Ciência e a Tecnologia (Portugal) within UID/AGR/00239/2013.

Disclosure statement

No potential conflict of interest was reported by the authors.

Funding

This work was supported by the Portuguese Science Foundation [SFRH/BD/52408/2013], Galician Government and European Social Fund: [Official Journal of Galicia – DOG No. 52, 17/03/2014], European Union's H2020 research and innovation program [Marie Sklodowska Curie Grant Agreement No. 691149].

References

Ahmed, O. S., A. Shemrock, D. Chabot, C. Dillon, G. Williams, R. Wasson, and S. E. Franklin. 2017. "Hierarchical Land Cover and Vegetation Classification Using Multispectral Data Acquired from an Unmanned Aerial Vehicle." *International Journal of Remote Sensing* 38 (8–10): 2037–2052. doi:10.1080/01431161.2017.1294781.

Baltsavias, E., A. Gruen, H. Eisenbeiss, L. Zhang, and L. T. Waser. 2008. "High-Quality Image Matching and Automated Generation of 3D Tree Models." *International Journal of Remote Sensing* 29 (5): 1243–1259. doi:10.1080/01431160701736513.

Baltsavias, E. P. 1999. "A Comparison between Photogrammetry and Laser Scanning." *ISPRS Journal of Photogrammetry and Remote Sensing* 54 (2): 83–94. doi:10.1016/S0924-2716(99)00014-3.

Bohlin, J., J. Wallerman, and J. E. S. Fransson. 2012. "Forest Variable Estimation Using Photogrammetric Matching of Digital Aerial Images in Combination with a High-Resolution DEM." *Scandinavian Journal of Forest Research* 27 (7): 692–699. doi:10.1080/02827581.2012.686625.

Bonnet, S., J. Lisein, and P. Lejeune. 2017. "Comparison of UAS Photogrammetric Products for Tree Detection and Characterization of Coniferous Stands." *International Journal of Remote Sensing* 38 (19): 5310–5337.

Dandois, J. P., and E. C. Ellis. 2010. "Remote Sensing of Vegetation Structure Using Computer Vision." *Remote Sensing* 2 (4): 1157–1176. doi:10.3390/rs2041157.

Dandois, J. P., and E. C. Ellis. 2013. "High Spatial Resolution Three-Dimensional Mapping of Vegetation Spectral Dynamics Using Computer Vision." *Remote Sensing of Environment* 136: 259–276. doi:10.1016/j.rse.2013.04.005.

Dandois, J. P., M. Olano, and E. C. Ellis. 2015. "Optimal Altitude, Overlap, and Weather Conditions for Computer Vision UAV Estimates of Forest Structure." *Remote Sensing* 7 (10): 13895–13920. doi:10.3390/rs71013895.

Dempewolf, J., J. Nagol, S. Hein, C. Thiel, and R. Zimmermann. 2017. "Measurement of Within-Season Tree Height Growth in a Mixed Forest Stand Using UAV Imagery." *Forests* 8 (7): 231. doi:10.3390/f8070231.

Díaz-Varela, R. A., R. de la Rosa, L. León, and P. J. Zarco-Tejada. 2015. "High-Resolution Airborne UAV Imagery to Assess Olive Tree Crown Parameters Using 3D Photo Reconstruction: Application in Breeding Trials." *Remote Sensing* 7 (4): 4213–4232. doi:10.3390/rs70404213.

Durrieu, S., C. Véga, M. Bouvier, F. Gosselin, J. P. Renaud, L. Saint-André, and P. S. Thenkabail. 2015. "Optical Remote Sensing of Tree and Stand Heights." In *Land Resources Monitoring, Modeling, and Mapping with Remote Sensing*, edited by Prasad S. Thenkabail, 449–485. Boca Raton, FL: CRC Press.

Estornell, J., L. A. Ruiz, B. Velázquez-Martí, and T. Hermosilla. 2011. "Analysis of the Factors Affecting LiDAR DTM Accuracy in a Steep Shrub Area." *International Journal of Digital Earth* 4 (6): 521–538. doi:10.1080/17538947.2010.533201.

Falkowski, M. J., A. M. S. Smith, P. E. Gessler, A. T. Hudak, L. A. Vierling, and J. S. Evans. 2008. "The Influence of Conifer Forest Canopy Cover on the Accuracy of Two Individual Tree Measurement Algorithms Using Lidar Data." *Canadian Journal of Remote Sensing* 34 (S2): S338–S350. doi:10.5589/m08-055.

Falkowski, M. J., J. S. Evans, S. Martinuzzi, P. E. Gessler, and A. T. Hudak. 2009. "Characterizing Forest Succession with Lidar Data: An Evaluation for the Inland Northwest, USA." *Remote Sensing of Environment* 113 (5): 946–956. doi:10.1016/j.rse.2009.01.003.

Franklin, S. E., and O. S. Ahmed. 2017. "Deciduous Tree Species Classification Using Object-Based Analysis and Machine Learning with Unmanned Aerial Vehicle Multispectral Data." *International Journal of Remote Sensing* 1–10. doi:10.1080/01431161.2017.1363442.

Fritz, A., T. Kattenborn, and B. Koch. 2013. "UAV-Based Photogrammetric Point Clouds—Tree Stem Mapping in Open Stands in Comparison to Terrestrial Laser Scanner Point Clouds." *International Archives Photogramm Remote Sens Spat Information Sciences* 40: 141–146. doi:10.5194/isprsarchives-XL-1-W2-141-2013.

Gatziolis, D., J. S. Fried, and V. S. Monleon. 2010. "Challenges to Estimating Tree Height via LiDAR in Closed-Canopy Forests: A Parable from Western Oregon." *Forest Science* 56 (2): 139–155.

Gonçalves-Seco, L., E. González-Ferreiro, U. Diéguez-Aranda, B. Fraga-Bugallo, R. Crecente, and D. Miranda. 2011. "Assessing the Attributes of High-Density Eucalyptus Globulus Stands Using Airborne Laser Scanner Data." *International Journal of Remote Sensing* 32 (24): 9821–9841. doi:10.1080/01431161.2011.593583.

González-Ferreiro, E., U. Diéguez-Aranda, L. Barreiro-Fernández, S. Buján, J. C. Miguel Barbosa, I. J. B. Suárez, and D. Miranda. 2013. "A Mixed Pixel-And Region-Based Approach for Using Airborne Laser Scanning Data for Individual Tree Crown Delineation in Pinus Radiata D. Don Plantations." *International Journal of Remote Sensing* 34 (21): 7671–7690. doi:10.1080/01431161.2013.823523.

Goodbody, T. R. H., N. C. Coops, P. Tompalski, P. Crawford, and K. J. K. Day. 2017c. "Updating Residual Stem Volume Estimates Using ALS-and UAV-Acquired Stereo-Photogrammetric Point Clouds." *International Journal of Remote Sensing* 38 (8–10): 2938–2953. doi:10.1080/01431161.2016.1219425.

Goodbody, T. R. H., N. C. Coops, P. L. Marshall, P. Tompalski, and P. Crawford. 2017b. "Unmanned Aerial Systems for Precision Forest Inventory Purposes: A Review and Case Study." *The Forestry Chronicle* 93 (1): 71–81. doi:10.5558/tfc2017-012.

Goodbody, T. R. H., N. C. Coops, T. Hermosilla, P. Tompalski, and P. Crawford. 2017a. "Assessing the Status of Forest Regeneration Using Digital Aerial Photogrammetry and Unmanned Aerial Systems." *International Journal of Remote Sensing* 1–19. doi:10.1080/01431161.2017.1402387.

Guerra-Hernández, J., E. González-Ferreiro, V. J. Monleón, S. P. Faias, M. Tomé, and R. A. Díaz-Varela. 2017. "Use of Multi-Temporal UAV-Derived Imagery for Estimating Individual Tree Growth in Pinus Pinea Stands." *Forests* 8 (8): 300. doi:10.3390/f8080300.

Guerra-Hernández, J., E. B. Görgens, J. García-Gutiérrez, L. C. E. Rodriguez, M. Tomé, and E. González-Ferreiro. 2016. "Comparison of ALS Based Models for Estimating Aboveground Biomass in Three Types of Mediterranean Forest." *European Journal of Remote Sensing* 49 (1): 185–204. doi:10.5721/EuJRS20164911.

Hirschmuller, H. 2005. "Accurate and Efficient Stereo Processing by Semi-Global Matching and Mutual Information." IEEE Computer Society Conference On Computer Vision and Pattern Recognition, 2005. CVPR 2005, vol. 2, 807–814. IEEE, San Diego, CA, June 20–25.

Holopainen, M., M. Vastaranta, M. Karjalainen, K. Karila, S. Kaasalainen, E. Honkavaara, and J. Hyyppä. 2015. "Forest Inventory Attribute Estimation Using Airborne Laser Scanning, Aerial Stereo Imagery, Radargrammetry and Interferometry-Finnish Experiences of the 3D Techniques." *ISPRS Annals of the Photogrammetry, Remote Sensing and Spatial Information Sciences* 2 (3): 63. doi:10.5194/isprsannals-II-3-W4-63-2015.

Hyyppä, J., H. Hyyppä, D. Leckie, F. Gougeon, X. Yu, and M. Maltamo. 2008. "Review of Methods of Small-Footprint Airborne Laser Scanning for Extracting Forest Inventory Data in Boreal Forests." *International Journal of Remote Sensing* 29 (5): 1339–1366. doi:10.1080/01431160701736489.

Hyyppä, J., and M. Inkinen. 1999. "Detecting and Estimating Attributes for Single Trees Using Laser Scanner." *The Photogrammetric Journal of Finland* 16 (2): 27–42.

Hyyppa, J., O. Kelle, M. Lehikoinen, and M. Inkinen. 2001. "A Segmentation-Based Method to Retrieve Stem Volume Estimates from 3-D Tree Height Models Produced by Laser Scanners." *IEEE Transactions on Geoscience and Remote Sensing* 39 (5): 969–975. doi:10.1109/36.921414.

Isenburg, M. 2016. *LAStools-Efficient Tools for LiDAR Processing. Version 161029*.

Jaakkola, A., J. Hyyppä, Y. Xiaowei, A. Kukko, H. Kaartinen, X. Liang, H. Hyyppä, and Y. Wang. 2017. "Autonomous Collection of Forest Field Reference—The Outlook and a First Step with UAV Laser Scanning." *Remote Sensing* 9 (8): 785. doi:10.3390/rs9080785.

Jensen, J. L. R., and A. J. Mathews. 2016. "Assessment of Image-Based Point Cloud Products to Generate a Bare Earth Surface and Estimate Canopy Heights in a Woodland Ecosystem." *Remote Sensing* 8 (1): 50. doi:10.3390/rs8010050.

Jiménez-Brenes, F. M., F. López-Granados, A. I. Castro, J. Torres-Sánchez, N. Serrano, and J. M. Peña. 2017. "Quantifying Pruning Impacts on Olive Tree Architecture and Annual Canopy Growth by Using UAV-Based 3D Modelling." *Plant Methods* 13 (1): 55. doi:10.1186/s13007-017-0205-3.

Kachamba, D. J., H. O. Ørka, E. Næsset, T. Eid, and T. Gobakken. 2017. "Influence of Plot Size on Efficiency of Biomass Estimates in Inventories of Dry Tropical Forests Assisted by Photogrammetric Data from an Unmanned Aircraft System." *Remote Sensing* 9 (6): 610. doi:10.3390/rs9060610.

Kattenborn, T., M. Sperlich, K. Bataua, and B. Koch. 2014. "Automatic Single Tree Detection in Plantations Using UAV-Based Photogrammetric Point Clouds." *The International Archives of Photogrammetry, Remote Sensing and Spatial Information Sciences* 40 (3): 139. doi:10.5194/isprsarchives-XL-3-139-2014.

Ke, Y., and L. J. Quackenbush. 2011. "A Review of Methods for Automatic Individual Tree-Crown Detection and Delineation from Passive Remote Sensing." *International Journal of Remote Sensing* 32 (17): 4725–4747. doi:10.1080/01431161.2010.494184.

Korpela, I. 2004. *Individual Tree Measurements by Means of Digital Aerial Photogrammetry*. Vol. 3. Finnish Society of Forest Science. Silvia Fennica. Monographs 3. https://helda.helsinki.fi/bitstream/handle/10138/20665/individu.pdf?sequence=2.

Laliberte, A. S., J. E. Herrick, A. Rango, and C. Winters. 2010. "Acquisition, Orthorectification, and Object-Based Classification of Unmanned Aerial Vehicle (UAV) Imagery for Rangeland Monitoring." *Photogrammetric Engineering & Remote Sensing* 76 (6): 661–672. doi:10.14358/PERS.76.6.661.

Leckie, D., F. Gougeon, D. Hill, R. Quinn, L. Armstrong, and R. Shreenan. 2003. "Combined High-Density Lidar and Multispectral Imagery for Individual Tree Crown Analysis." *Canadian Journal of Remote Sensing* 29 (5): 633–649. doi:10.5589/m03-024.

Lim, K., P. Treitz, M. Wulder, B. St-Onge, and M. Flood. 2003. "LiDAR Remote Sensing of Forest Structure." *Progress in Physical Geography* 27 (1): 88–106. doi:10.1191/0309133303pp360ra.

Lindberg, E., and M. Hollaus. 2012. "Comparison of Methods for Estimation of Stem Volume, Stem Number and Basal Area from Airborne Laser Scanning Data in a Hemi-Boreal Forest." *Remote Sensing* 4 (4): 1004–1023. doi:10.3390/rs4041004.

Lisein, J., M. Pierrot-Deseilligny, S. Bonnet, and P. Lejeune. 2013. "A Photogrammetric Workflow for the Creation of A Forest Canopy Height Model from Small Unmanned Aerial System Imagery." *Forests* 4 (4): 922–944. doi:10.3390/f4040922.

McGaughey, R. 2016. "FUSION/LDV: Software for LiDAR Data Analysis and Visualization. Version 3.41. Seattle, WA: US Department of Agriculture, Forest Service." *Pacific Northwest Research Station*.

Mohan, M., C. A. Silva, C. Klauberg, P. Jat, G. Catts, A. Cardil, A. T. Hudak, and M. Dia. 2017. "Individual Tree Detection from Unmanned Aerial Vehicle (UAV) Derived Canopy Height Model in an Open Canopy Mixed Conifer Forest." *Forests* 8 (9): 340. doi:10.3390/f8090340.

Naesset, E. 1997. "Estimating Timber Volume of Forest Stands Using Airborne Laser Scanner Data." *Remote Sensing of Environment* 61 (2): 246–253. doi:10.1016/S0034-4257(97)00041-2.

Næsset, E. 2002. "Predicting Forest Stand Characteristics with Airborne Scanning Laser Using a Practical Two-Stage Procedure and Field Data." *Remote Sensing of Environment* 80 (1): 88–99. doi:10.1016/S0034-4257(01)00290-5.

Næsset, E., O. M. Bollandsås, and T. Gobakken. 2005. "Comparing Regression Methods in Estimation of Biophysical Properties of Forest Stands from Two Different Inventories Using Laser Scanner Data." *Remote Sensing of Environment* 94 (4): 541–553. doi:10.1016/j.rse.2004.11.010.

Näsi, R., E. Honkavaara, P. Lyytikäinen-Saarenmaa, M. Blomqvist, P. Litkey, T. Hakala, N. Viljanen, T. Kantola, T. Tanhuanpää, and M. Holopainen. 2015. "Using UAV-Based Photogrammetry and Hyperspectral Imaging for Mapping Bark Beetle Damage at Tree-Level." *Remote Sensing* 7 (11): 15467–15493. doi:10.3390/rs71115467.

Nevalainen, O., E. Honkavaara, S. Tuominen, N. Viljanen, T. Hakala, Y. Xiaowei, J. Hyyppä, H. Saari, I. Pölönen, and N. N. Imai. 2017. "Individual Tree Detection and Classification with UAV-Based Photogrammetric Point Clouds and Hyperspectral Imaging." *Remote Sensing* 9 (3): 185. doi:10.3390/rs9030185.

Nurminen, K., M. Karjalainen, Y. Xiaowei, J. Hyyppä, and E. Honkavaara. 2013. "Performance of Dense Digital Surface Models Based on Image Matching in the Estimation of Plot-Level Forest Variables." *ISPRS Journal of Photogrammetry and Remote Sensing* 83: 104–115. doi:10.1016/j.isprsjprs.2013.06.005.

Panagiotidis, D., A. Abdollahnejad, P. Surový, and V. Chiteculo. 2017. "Determining Tree Height and Crown Diameter from High-Resolution UAV Imagery." *International Journal of Remote Sensing* 38 (8–10): 2392–2410.

Popescu, S. C. 2007. "Estimating Biomass of Individual Pine Trees Using Airborne Lidar." *Biomass and Bioenergy* 31 (9): 646–655. doi:10.1016/j.biombioe.2007.06.022.

Popescu, S. C., R. H. Wynne, and R. F. Nelson. 2003. "Measuring Individual Tree Crown Diameter with Lidar and Assessing Its Influence on Estimating Forest Volume and Biomass." *Canadian Journal of Remote Sensing* 29 (5): 564–577. doi:10.5589/m03-027.

Popescu, S. C., R. H. Wynne, and J. A. Scrivani. 2004. "Fusion of Small-Footprint Lidar and Multispectral Data to Estimate Plot-level Volume and Biomass in Deciduous and Pine Forests in Virginia, USA." *Forest Science* 50 (4): 551–565.

Puliti, S., H. O. Ørka, T. Gobakken, and N. Erik. 2015. "Inventory of Small Forest Areas Using an Unmanned Aerial System." *Remote Sensing* 7 (8): 9632–9654. doi:10.3390/rs70809632.

Puliti, S., L. T. Ene, T. Gobakken, and N. Erik. 2017a. "Use of Partial-Coverage UAV Data in Sampling for Large Scale Forest Inventories." *Remote Sensing of Environment* 194: 115–126. doi:10.1016/j.rse.2017.03.019.

Puliti, S., T. Gobakken, H. O. Ørka, and N. Erik. 2017b. "Assessing 3D Point Clouds from Aerial Photographs for Species-Specific Forest Inventories." *Scandinavian Journal of Forest Research* 32 (1): 68–79. doi:10.1080/02827581.2016.1186727.

Puttonen, E., P. Litkey, and J. Hyyppä. 2009. "Individual Tree Species Classification by Illuminated—Shaded Area Separation." *Remote Sensing* 2 (1): 19–35. doi:10.3390/rs2010019.

Raber, G. T., J. R. Jensen, S. R. Schill, and K. Schuckman. 2002. "Creation of Digital Terrain Models Using an Adaptive Lidar Vegetation Point Removal Process." *Photogrammetric Engineering and Remote Sensing* 68 (12): 1307–1314.

Rahlf, J., J. Breidenbach, S. Solberg, E. Næsset, and R. Astrup. 2014. "Comparison of Four Types of 3D Data for Timber Volume Estimation." *Remote Sensing of Environment* 155: 325–333. doi:10.1016/j.rse.2014.08.036.

Silva, C. A., A. T. Hudak, L. A. Vierling, E. Louise Loudermilk, J. J. O'Brien, J. Kevin Hiers, S. B. Jack, C. Gonzalez-Benecke, H. Lee, and M. J. Falkowski. 2016. "Imputation of Individual Longleaf Pine (Pinus Palustris Mill.) Tree Attributes from Field and LiDAR Data." *Canadian Journal of Remote Sensing* 42 (5): 554–573. doi:10.1080/07038992.2016.1196582.

Simic Milas, Anita, K. Arend, C. Mayer, Martin Simonson, and S. Mackey. 2017. "Different Colours of Shadows: Classification of UAV Images." *International Journal of Remote Sensing* 38 (8–10): 3084–3100. doi:10.1080/01431161.2016.1274449.

Solberg, S., E. Naesset, and O. M. Bollandsas. 2006. "Single Tree Segmentation Using Airborne Laser Scanner Data in a Structurally Heterogeneous Spruce Forest." *Photogrammetric Engineering & Remote Sensing* 72 (12): 1369–1378. doi:10.14358/PERS.72.12.1369.

Sperlich, M., T. Kattenborn, B. Koch, and G. Kattenborn. 2014. "Potential of Unmanned Aerial Vehicle Based Photogrammetric Point Clouds for Automatic Single Tree Detection." Accessed 15 January 2015.. Http://Www.Dgpf.de/Neu/Proc2014/Proceedings/Papers/Beitrag270.Pdf.

St-Onge, B., C. Vega, R. A. Fournier, and Y. Hu. 2008. "Mapping Canopy Height Using a Combination of Digital Stereo-Photogrammetry and Lidar." *International Journal of Remote Sensing* 29 (11): 3343–3364. doi:10.1080/01431160701469040.

St-Onge, B., J. Jumelet, M. Cobello, and V. Cédric. 2004. "Measuring Individual Tree Height Using a Combination of Stereophotogrammetry and Lidar." *Canadian Journal of Forest Research* 34 (10): 2122–2130. doi:10.1139/x04-093.

Suárez, J. C., C. Ontiveros, S. Smith, and S. Snape. 2005. "Use of Airborne LiDAR and Aerial Photography in the Estimation of Individual Tree Heights in Forestry." *Computers & Geosciences* 31 (2): 253–262. doi:10.1016/j.cageo.2004.09.015.

Tanhuanpää, T., N. Saarinen, V. Kankare, K. Nurminen, M. Vastaranta, E. Honkavaara, M. Karjalainen, Y. Xiaowei, M. Holopainen, and H. Juha. 2016. "Evaluating the Performance of High-Altitude Aerial Image-Based Digital Surface Models in Detecting Individual Tree Crowns in Mature Boreal Forests." *Forests* 7 (7): 143. doi:10.3390/f7070143.

Thiel, C., and C. Schmullius. 2017. "Comparison of UAV Photograph-Based and Airborne Lidar-Based Point Clouds over Forest from a Forestry Application Perspective." *International Journal of Remote Sensing* 38 (8–10): 2411–2426. doi:10.1080/01431161.2016.1225181.

Tomaštík, J., M. Mokroš, Š. Saloň, F. Chudý, and T. Daniel. 2017. "Accuracy of Photogrammetric UAV-Based Point Clouds under Conditions of Partially-Open Forest Canopy." *Forests* 8 (5): 151. doi:10.3390/f8050151.

Torresan, C., A. Berton, F. Carotenuto, S. F. Di Gennaro, B. Gioli, A. Matese, F. Miglietta, C. Vagnoli, A. Zaldei, and L. Wallace. 2017. "Forestry Applications of UAVs in Europe: A Review." *International Journal of Remote Sensing* 38 (8–10): 2427–2447.

Vastaranta, M., M. A. Wulder, J. C. White, A. Pekkarinen, S. Tuominen, C. Ginzler, V. Kankare, M. Holopainen, J. Hyyppä, and H. Hannu. 2013. "Airborne Laser Scanning and Digital Stereo Imagery Measures of Forest Structure: Comparative Results and Implications to Forest Mapping and Inventory Update." *Canadian Journal of Remote Sensing* 39 (5): 382–395. doi:10.5589/m13-046.

Vauhkonen, J., L. Ene, S. Gupta, J. Heinzel, J. Holmgren, J. Pitkänen, S. Solberg, Y. Wang, H. Weinacker, and K. Marius Hauglin. 2011. "Comparative Testing of Single-Tree Detection Algorithms under Different Types of Forest." *Forestry* 85 (1): 27–40. doi:10.1093/forestry/cpr051.

Wack, R., M. Schardt, U. Lohr, L. Barrucho, and T. Oliveira. 2003. "Forest Inventory for Eucalyptus Plantations Based on Airborne Laserscanner Data." *International Archives of Photogrammetry and Remote Sensing* 34 (part 3): W13.

Wallace, L., A. Lucieer, C. Watson, and D. Turner. 2012. "Development of a UAV-LiDAR System with Application to Forest Inventory." *Remote Sensing* 4 (6): 1519–1543. doi:10.3390/rs4061519.

Wallace, L., A. Lucieer, Z. Malenovský, D. Turner, and V. Petr. 2016. "Assessment of Forest Structure Using Two UAV Techniques: A Comparison of Airborne Laser Scanning and Structure from Motion (Sfm) Point Clouds." *Forests* 7 (3): 62. doi:10.3390/f7030062.

Westoby, M. J., J. Brasington, N. F. Glasser, M. J. Hambrey, and J. M. Reynolds. 2012. "'Structure-From-Motion'photogrammetry: A Low-Cost, Effective Tool for Geoscience Applications." *Geomorphology* 179: 300–314. doi:10.1016/j.geomorph.2012.08.021.

White, J. C., C. Stepper, P. Tompalski, N. C. Coops, and M. A. Wulder. 2015. "Comparing ALS and Image-Based Point Cloud Metrics and Modelled Forest Inventory Attributes in a Complex Coastal Forest Environment." *Forests* 6 (10): 3704–3732. doi:10.3390/f6103704.

White, J. C., M. A. Wulder, N. C. Mikko Vastaranta, D. P. Coops, and M. Woods. 2013. "The Utility of Image-Based Point Clouds for Forest Inventory: A Comparison with Airborne Laser Scanning." *Forests* 4 (3): 518–536. doi:10.3390/f4030518.

White, J. C., N. C. Coops, M. A. Wulder, M. Vastaranta, T. Hilker, and P. Tompalski. 2016. "Remote Sensing Technologies for Enhancing Forest Inventories: A Review." *Canadian Journal of Remote Sensing* 42 (5): 619–641.

Wulder, M. K., O. Niemann, and D. G. Goodenough. 2000. "Local Maximum Filtering for the Extraction of Tree Locations and Basal Area from High Spatial Resolution Imagery." *Remote Sensing of Environment* 73 (1): 103–114. doi:10.1016/S0034-4257(00)00101-2.

Zarco-Tejada, P. J., R. Diaz-Varela, V. Angileri, and P. Loudjani. 2014. "Tree Height Quantification Using Very High Resolution Imagery Acquired from an Unmanned Aerial Vehicle (UAV) and Automatic 3D Photo-Reconstruction Methods." *European Journal of Agronomy* 55: 89–99. doi:10.1016/j.eja.2014.01.004.